

$K \rightarrow \pi\pi$ decay matrix elements at the physical point with periodic boundary conditions

Masaaki Tomii,^{a,*} Thomas Blum,^{a,b} Daniel Hoyer,^c Taku Izubuchi,^{b,d}
Luchang Jin,^{a,b} Chulwoo Jung^d and Amarjit Soni^d

^aPhysics Department, University of Connecticut, Storrs, CT 06269, USA

^bRIKEN-BNL Research Center, Brookhaven National Laboratory, Upton, NY 11973, USA

^cDepartment of Computational Mathematics, Science and Engineering, and Department of Physics and Astronomy, Michigan State University, East Lansing, MI, 48824, USA

^dPhysics Department, Brookhaven National Laboratory, Upton, NY 11973, USA

E-mail: masaaki.tomii@uconn.edu

We calculate $K \rightarrow \pi\pi$ matrix elements using periodic boundary conditions as an independent calculation from our previous study with G-parity boundary conditions. We present our preliminary results for $K \rightarrow \pi\pi$ three-point functions and matrix elements on a 24^3 , $a^{-1} = 1$ GeV, 2 + 1-flavor Möbius DWF ensemble at physical pion and kaon masses generated by the RBC and UKQCD collaborations and discuss the prospect for high-precision computation of ε' with periodic boundary conditions.

*The 38th International Symposium on Lattice Field Theory, LATTICE2021 26th-30th July, 2021
Zoom/Gather@Massachusetts Institute of Technology*

*Speaker

1. Introduction

Direct CP violation in $K \rightarrow \pi\pi$ decays, which is parametrized by ε' , attracts close attention from particle phenomenologists. Since it is highly suppressed in the Standard Model, it is expected to be a rich probe for searching new physics beyond the Standard Model.

With various improvements to our first result for ε' [1], we have completed our calculation on a single lattice ensemble with G-parity boundary conditions [2]. Our result is $\text{Re}(\varepsilon'/\varepsilon)_{\text{SM}} = 21.7(2.6)(6.2)(5.0) \times 10^{-4}$, where ε is the measure of indirect CP violation and the first two errors represent statistical and systematic in our lattice calculation. The third error corresponds to omitted isospin breaking and QED corrections. While this result is consistent with the average of the experimental results $\text{Re}(\varepsilon'/\varepsilon)_{\text{exp}} = 16.6(2.3) \times 10^{-4}$ [3, 4], more independent calculations with better precision would be desired.

The major sources of systematic error in our previous calculation are 1. truncation error of perturbative matching of the Wilson coefficients between four- and three-flavor theories at the charm threshold, 2. finite lattice cutoff effects and 3. isospin breaking and QED corrections. For the matching of the Wilson coefficients, we are attempting to implement a nonperturbative procedure [5] instead of the perturbative approach.

The other two sources of systematic uncertainty listed above motivate us to calculate the $K \rightarrow \pi\pi$ matrix elements with periodic boundary conditions. For finite lattice cutoff effects, while we are generating finer G-parity ensembles to take the continuum limit within the calculation with G-parity boundary conditions, we can perform an independent calculation with periodic boundary conditions with the ensembles with various lattice spacings that we have already generated. Also, it is more straightforward for periodic boundary conditions to introduce isospin breaking and QED effects than G-parity boundary conditions. Thus our study would give us the prospect of obtaining ε' more precisely.

It is challenging to extract the on-shell kinematics of $K \rightarrow \pi\pi$ from euclidean three-point functions with periodic boundary conditions because of the presence of the off-shell two-pion state with the energy $E_{\pi\pi} \simeq 2m_\pi$, which is smaller than that of the on-shell kinematics $E_{\pi\pi} = m_K$. It also turned out that the contamination from heavier two-pion states are significant [2, 6]. Therefore we seriously perform state decomposition by solving the generalized eigenvalue problem (GEVP) [7, 8] to well extract the on-shell kinematics of $K \rightarrow \pi\pi$ decays.

In this article we give our preliminary results for the $K \rightarrow \pi\pi$ three-point functions and matrix elements calculated on the $24^3 \times 64$ lattice ensemble with 2+1-flavor Möbius domain-wall fermions near the physical pion and kaon masses and the lattice cutoff $a^{-1} \simeq 1$ GeV. The measurements are done with 258 configurations. We use all-to-all quark propagators with 2,000 low modes from the Lanczos algorithm for the light quark and spin-color-time diluted CG inversions with random noise vectors for both the light and strange quarks.

2. Correlation functions

In order to obtain the $K \rightarrow \pi\pi$ matrix elements, we need to calculate two-point functions of interpolation operators as well as three-point functions of the interpolation operators and the $\Delta S = 1$ four-quark effective operators. The following subsections explain these correlation functions.

2.1 Two-point function of kaon operator

The simplest correlation function is the two-point function of a kaon interpolation operator

$$C^K(t) = \langle O_K(t)^\dagger O_K(0) \rangle. \quad (1)$$

We perform the exponential smearing for the kaon interpolation operator with the radius of 2 in lattice units.

2.2 Two-point functions of two-pion operators

We employ multiple two-pion interpolation operators

$$O_{\pi\pi,\alpha}(t) \in \{\pi\pi(000), \pi\pi(001), \pi\pi(011), \pi\pi(111), \sigma\}, \quad (2)$$

where $\pi\pi(abc)$ with $a, b, c = 0, 1$ is a product of two pion interpolation operators with the momenta indicated by (abc) . The number of the 1's in abc indicates the number of directions to which each pion interpolation operator has one unit of momentum $\pm 2\pi/L$. One of the pion interpolation operators has the opposite momentum to the other's, i.e. we employ the center of mass frame. We use neutral isospin-definite two-pion operators, which can be constructed by an appropriate linear combination of $\pi^+\pi^-$, $\pi^0\pi^0$ and $\pi^-\pi^+$. For the $I = 0$ channel, we also employ σ as a two-pion interpolation operator. We perform the exponential smearing for the pion and sigma operators with the radius of 1.5 in lattice units.

We calculate two-point functions of these two-pion operators

$$C_{\alpha\beta}^{\pi\pi}(t) = \langle O_{\pi\pi,\alpha}(t)^\dagger O_{\pi\pi,\beta}(0) \rangle - \langle O_{\pi\pi,\alpha}^\dagger \rangle \langle O_{\pi\pi,\beta} \rangle, \quad (3)$$

where the second term on the right hand side is the vacuum subtraction term needed for the $I = 0$ channel. In order to extract the signal from a certain state, we solve the generalized eigenvalue problem (GEVP) [7]

$$\sum_{\beta} C_{\alpha\beta}^{\pi\pi}(t) v_{n,\beta}(t, t_0) = \lambda_n(t, t_0) \sum_{\beta} C_{\alpha\beta}^{\pi\pi}(t_0) v_{n,\beta}(t, t_0), \quad (4)$$

where $\lambda_n(t, t_0)$ is an eigenvalue of the GEVP and $v_{n,\beta}(t, t_0)$ is the corresponding eigenvector. We use $t_0 = t - 1$ in this work. Preliminary results for our GEVP analysis are presented in Ref. [9].

2.3 $K \rightarrow \pi\pi$ three-point functions

We calculate $K \rightarrow \pi\pi$ three-point functions

$$C_{\alpha,i}^{3\text{pt}}(t_1, t_2) = \langle O_{\pi\pi,\alpha}(t_{\pi\pi})^\dagger Q_i(t_{op}) O_K(t_K) \rangle, \quad t_1 = t_{\pi\pi} - t_{op}, t_2 = t_{op} - t_K, \quad (5)$$

where each operator is summed over spatial volume and Q_i is the $\Delta S = 1$ four-quark operators [10] relevant for $K \rightarrow \pi\pi$ decays. Wick contractions of these correlation functions yield four typical diagrams shown in Figure 1. We name these diagrams *type1* through *type4*. While the $I = 2$ channel only has the contribution from the *type1*, we need to calculate the four diagrams for the $I = 0$ channel. For the $K \rightarrow \sigma$ correlation functions, there are the diagrams that are analogous to the *type2–4* diagrams.

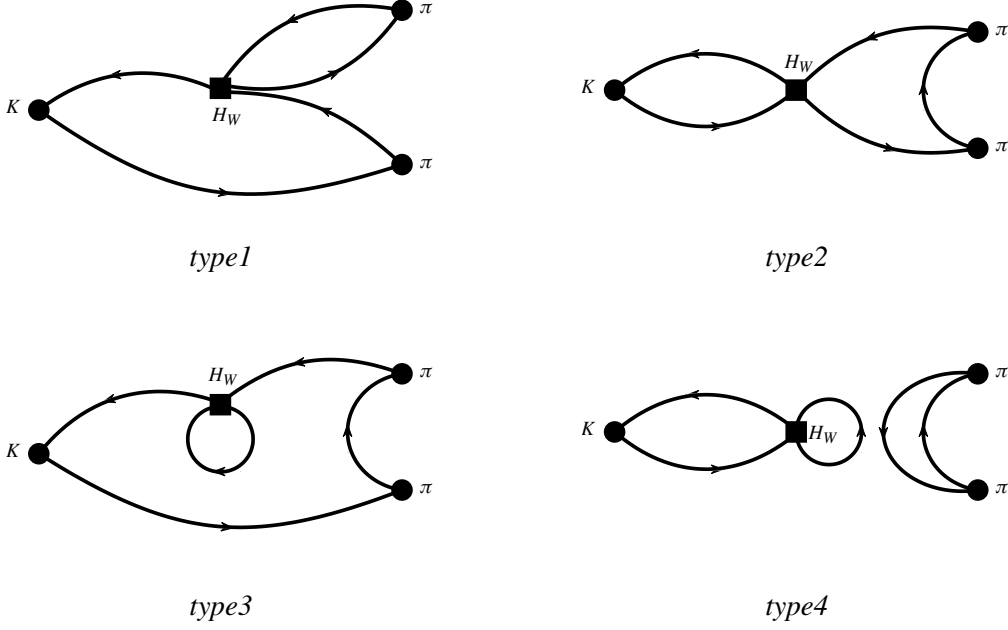


Figure 1: Diagrams that contribute to $K \rightarrow \pi\pi$ three-point functions.

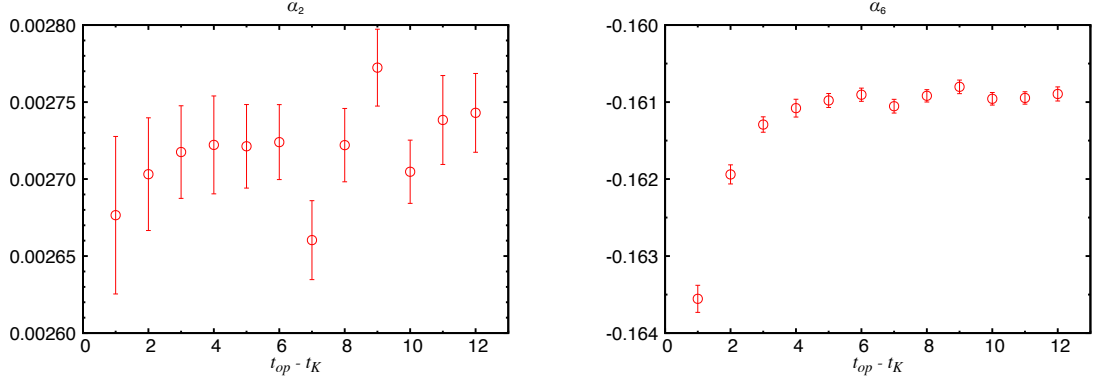


Figure 2: Subtraction coefficients α_2 (left) and α_6 (right) for Q_2 and Q_6 , respectively.

The presence of a quark loop in the *type3* and *type4* diagrams induces a power divergence, which needs to be removed by defining the subtracted four-quark operators

$$Q_i = \hat{Q}_i - \alpha_i \bar{s} \gamma_5 d, \quad (6)$$

with the unsubtracted four-quark operators \hat{Q}_i . We determine the subtraction coefficients α_i by imposing the condition

$$\langle Q_i(t_{op}) O_K(t_K) \rangle = 0. \quad (7)$$

Figure 2 shows preliminary results for α_2 (left) and α_6 (right). We use these time-dependent subtraction coefficients for calculating the three-point functions with the subtracted four-quark

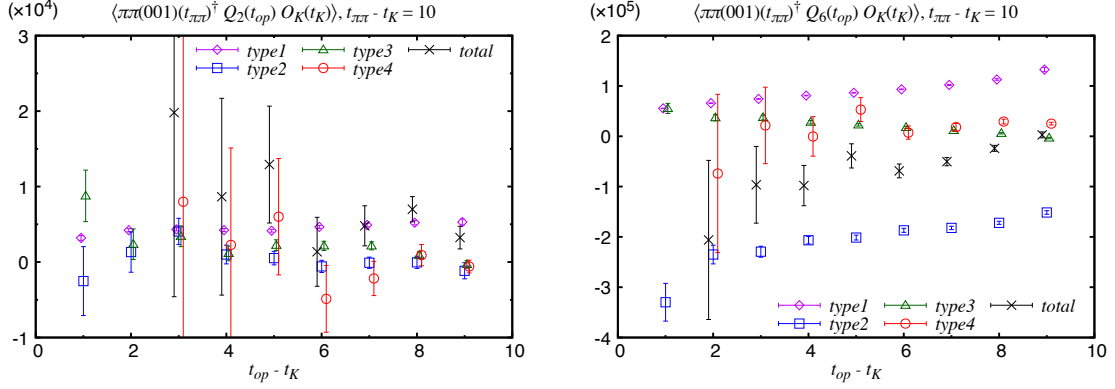


Figure 3: $K \rightarrow \pi\pi$ correlation functions with the four-quark operators Q_2 (left) and Q_6 (right) and the $I = 0$ two-pion operator $\pi\pi(001)$ at $t_{\pi\pi} - t_K = 10$ and their breakdowns into the contributions of each diagram.

operators, i.e. we calculate the three-point functions at $t_2 = t_{op} - t_K$ using the subtraction coefficients calculated at the same time separation $t_2 = t_{op} - t_K$. This subtraction condition also removes the vacuum term $\langle O_{\pi\pi,\alpha}^\dagger \langle Q_i(t_{op}) O_K(t_K) \rangle \rangle$ that could arise in the $K \rightarrow \pi\pi$ three-point functions (5) if a different subtraction condition was imposed. In what follows, the four-quark operators are understood as the subtracted ones.

The computational cost of the *type1* and *type2* diagrams is as high as that of A2A propagators and much higher than that of *type3* and *type4*. Since the *type4* diagram, which is disconnected, is expected and verified [2] to dominates the statistical error of the $I = 0$ channel of the three-point functions, the number of measurements of *type1* and *type2* diagrams can be reduced without spoiling the statistical precision. We perform the cost reduction by reducing the number of lattice sites of the four-quark operators from 24^3 to 8^3 for each time slice. With this reduction we can in principle take the contractions of *type1* and *type2* diagrams $27\times$ faster.

Figure 3 shows the $K \rightarrow \pi\pi$ three-point functions with the four-quark operators Q_2 (left) and Q_6 (right) and the $I = 0$ two-pion operator $\pi\pi(001)$, which couples well with the first excited two-pion state, which describes nearly on-shell kinematics in our lattice setup. The figure also shows the breakdown of the correlation functions into the contributions of each diagram. According to our $\pi\pi$ scattering study [9], the contaminations from higher excited states that are not taken into account by the GEVP approach is significant at time separation 1 and 2 in lattice units and therefore we expect we need to extract the $K \rightarrow \pi\pi$ matrix elements in the region $t_{\pi\pi} - t_{op} \geq 3$, where the statistical error is dominated by the *type4* diagram. Thus the cost reduction of the *type1* and *type2* diagrams does not appear to affect the statistical precision and therefore is successful.

3. Effective matrix elements

Following the discussion in Ref. [8], we calculate the $K \rightarrow \pi\pi$ effective matrix elements

$$M_{i,n}^{eff}(t_1, t_2) = \frac{\tilde{C}_{n,i}^{3pt}(t_1, t_2)}{\sqrt{\lambda_n^{t_1} e^{-m_K t_2} \tilde{C}_n^{\pi\pi}(t_1) C^K(t_2)}}, \quad (8)$$

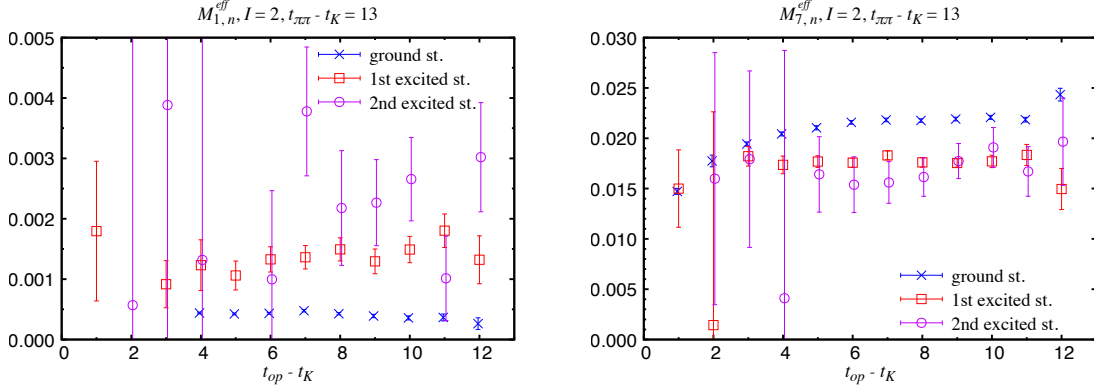


Figure 4: Preliminary results for $K \rightarrow \pi\pi$ effective matrix elements with the four-quark operators Q_1 (left) and Q_7 (right) and the $I = 2$ two-pion operators. Here the two-pion operators $\pi\pi(000)$, $\pi\pi(001)$, $\pi\pi(011)$ and $\pi\pi(111)$ are used for GEVP.

where we define state-projected correlation functions

$$\tilde{C}_{n,i}^{3pt}(t_1, t_2) = \sum_{\alpha} v_{n,\alpha}^* C_{\alpha,i}^{3pt}(t_1, t_2), \quad (9)$$

$$\tilde{C}_n^{\pi\pi}(t_1) = \sum_{\alpha,\beta} v_{n,\alpha}^* C_{\alpha\beta}^{\pi\pi}(t_1) v_{n,\beta}, \quad (10)$$

with λ_n and $v_{n,\alpha}$ being the eigenvalues and eigenvectors extracted from a plateau region of the GEVP effective energies for the two-pion correlation functions.

Figure 4 shows the $I = 2$ channel of the effective matrix elements with the four-quark operators Q_1 (left) and Q_7 (right). We solve GEVP with the four two-pion interpolation operators $\pi\pi(000)$, $\pi\pi(001)$, $\pi\pi(011)$ and $\pi\pi(111)$. While the third excited two-pion state is also included in this GEVP analysis, the corresponding matrix element is omitted from the plots since it has a large statistical error. We see a good plateau on the effective matrix elements with the first excited two-pion state (squares), which describes nearly on-shell kinematics.

Figure 5 shows the $I = 0$ channel of the effective matrix elements with the four-quark operators Q_2 (left) and Q_6 (right). Here, the three two-pion interpolation operators $\pi\pi(000)$, $\pi\pi(001)$ and σ are used for the GEVP analysis. While the $I = 0$ channel is noisier than the $I = 2$ channel because of the presence of a disconnected diagram and we may need to increase the statistics and improve the analysis, we still see some signal and plateau, which indicate the feasibility of calculating the $I = 0$ channel of $K \rightarrow \pi\pi$ matrix elements and ε' with periodic boundary conditions.

4. Summary

This study gives us a prospect that we could successfully calculate the $K \rightarrow \pi\pi$ matrix elements and ε' with periodic boundary conditions. We are attempting to decrease the statistical error by the factor of 3 in order to reach the same precision as the one we had in our previous calculation with G-parity boundary conditions [2]. While we apply the AMA correction to the correlation

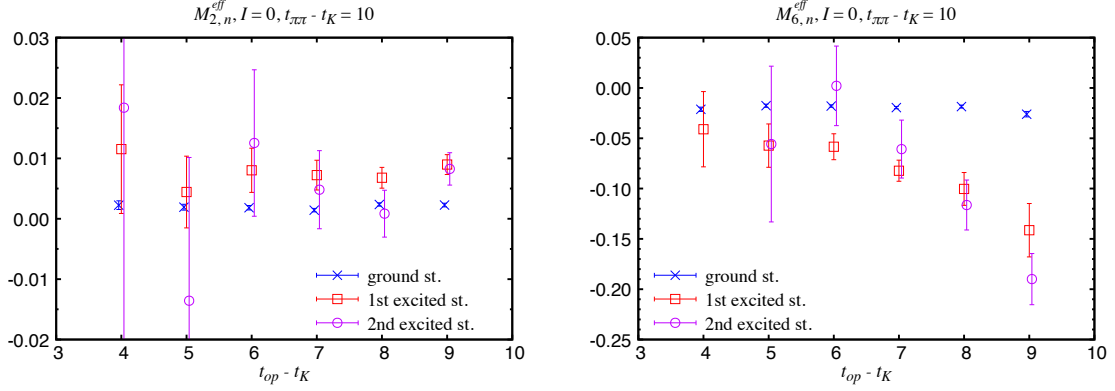


Figure 5: Preliminary results for $K \rightarrow \pi\pi$ effective matrix elements with the four-quark operators Q_2 (left) and Q_6 (right) and the $I = 0$ two-pion operators. Here the three two-pion operators $\pi\pi(000)$, $\pi\pi(001)$ and σ are used for GEVP.

functions of two-pion operators, we have not introduced it to the $K \rightarrow \pi\pi$ three-point functions. This makes the jackknife analysis nontrivial about noise cancelation due to the correlation between the numerator and denominator of Eq. (8). We are close to introduce the AMA correction to the three-point functions and see how it improves the precision.

Acknowledgments

M.T, T.B and L.C.J were supported in part by US DOE grant DE-SC0010339. M.T. and L.C.J. were also supported in part by DOE Office of Science Early Career Award DE-SC0021147. D.H was supported in part by a SCIDAC grant “Computing the Properties of Matter with Leadership Computing Resources.” T.I, C.J and A.S were supported in part by US DOE grant DE-SC0012704. Computations for this work were carried out on facilities of the USQCD Collaboration, which are funded by the Office of Science of the U.S. Department of Energy.

References

- [1] Z. Bai *et al.* [RBC and UKQCD], Phys. Rev. Lett. **115**, no.21, 212001 (2015) [arXiv:1505.07863 [hep-lat]].
- [2] R. Abbott *et al.* [RBC and UKQCD], Phys. Rev. D **102**, no.5, 054509 (2020) [arXiv:2004.09440 [hep-lat]].
- [3] J. R. Batley *et al.* [NA48], Phys. Lett. B **544**, 97-112 (2002) [arXiv:hep-ex/0208009 [hep-ex]].
- [4] E. Abouzaid *et al.* [KTeV], Phys. Rev. D **83**, 092001 (2011) [arXiv:1011.0127 [hep-ex]].
- [5] M. Tomii, PoS LATTICE2019, 174 (2020)
- [6] T. Blum *et al.* [RBC and UKQCD], Phys. Rev. D **104**, no.11, 114506 (2021) [arXiv:2103.15131 [hep-lat]].

- [7] B. Blossier, M. Della Morte, G. von Hippel, T. Mendes and R. Sommer, JHEP **04**, 094 (2009) [arXiv:0902.1265 [hep-lat]].
- [8] J. Bulava, M. Donnellan and R. Sommer, JHEP **01**, 140 (2012) [arXiv:1108.3774 [hep-lat]].
- [9] D. Hoying, PoS **LATTICE2019**, 268 (2020)
- [10] A. J. Buras, M. Jamin and M. E. Lautenbacher, Nucl. Phys. B **408**, 209-285 (1993) [arXiv:hep-ph/9303284 [hep-ph]].